Size effects in the fatigue behavior of welded steel tubular bridge joints

Größeneffekte beim Ermüdungsverhalten von geschweißten kreisförmigen Stahlhohlprofilverbindungen für den Brückenbau

A. Nussbaumer, L. A. Costa Borges

Tubular space trusses for bridge applications use thick-walled tubes. The reduction in fatigue resistance due to geometrical size effects is thus an important issue. In order to carry out a thorough study, both fatigue tests on large-scale specimens and advanced 3D crack propagation modelling were carried out at ICOM/EPFL. The study is limited to circular hollow sections (CHS) K-joints. An alternate current potential drop (ACPD) system is used to measure crack depth on nodes of the tested truss specimens. The results obtained from the tests are given in the paper in terms of S-N data, crack depth versus number of cycles and deduced crack propagation rates. The numerical model was developed using the dual boundary elements method (DBEM), software BEASY^{TM}, and was validated with fatigue tests data. The stress intensity factors (SIF) along the doubly curved crack front at different crack depths were obtained. With this model, a parametric study investigates the influence of geometry, size and load case on fatigue life. The results of both proportional and non-proportional sizing effects on fatigue strength are presented. The paper shows that size effects (proportional and non-proportional) can be expressed as a function of the non-dimensional parameters and chord thickness.

Keywords: Structural steel, fatigue, size effects, large-scale tests, boundary element method.

Im Brückenbau werden Raumfachwerke aus geschweißten Stahlhohlprofilen eingesetzt. Aufgrund der Bauteilabmessungen muss dem schwingfestigkeitsmindernden Größeneffekt besonders Rechnung getragen werden. In einer diesbezüglichen, gründlichen Studie wurden am ICOM/EPFL sowohl Ermüdungsversuche an großmaßstäblichen Proben als auch fortschrittliche Modellierungen des 3D-Ermüdungsrissfortschritts durchgeführt. Die Studie ist auf kreisförmige K-Rohrknoten (CHS) beschränkt. Die Risstiefen an den Schweißnahtübergangskerben wurden mit dem Wechselstrompotenzial-Verfahren (ACPD) gemessen. Die Ergebnisse werden hier als Wöhlerlinien, Rissfortschrittskurven und daraus abgeleiteten Kurven für die Risswachstumsrate mitgeteilt. Das Risswachstum wurde unter Zuhilfenahme der dualen Randelementemethode, Software BEASY^{TM}, modelliert, wodurch die Versuchsergebnisse untermauert werden konnten. Insbesondere wurden die Spannungsintensitätsfaktoren (SIF) entlang der doppelt gekrümmten Rissfront für verschiedene Risstiefen berechnet. In einer parametrischen Studie mit diesem Modell wurden die Einflüsse der Geometrie, der Größe und der Lastkonfiguration auf die Lebensdauer untersucht. Diese Ergebnisse werden hier sowohl für proportionale als auch für nichtproportionale Größeneffekte vorgestellt. In der vorliegenden Veröffentlichung wird gezeigt, dass die Größeneffekte (proportional und nichtproportional) als Funktion von dimensionslosen Parametern und von der Gurtblechdicke beschrieben werden können.

Schlüsselworte: Baustahl, Ermüdung, Größeneffekt, großmaßstäbliche Versuche, Randelement-Methode.

1 Introduction

1.1 Welded tubular bridge fatigue design

In welded tubular truss bridges, rectangular or circular hollow sections (RHS, CHS) with low values of the ratio diameter to thickness are usually preferred. It results from the will to best satisfy both the constraints of high forces, fatigue loadings and truss transparency for keeping good aesthetics. Since fatigue is a dominant design criterion for welded joints in CHS, significant work has gone into the development of design methodologies and guidelines for the fatigue behaviour of welded tubular joints (CIDECT 2000, IIW 2000) [1, 2]. The fatigue strength of a tubular structure depends both on the absolute as well as on the relative size of its members. The current approach to account for size effects for tubes in various structural applications has limitations, in particular due to differences in the loading cases and can be very penalizing for the thick-walled tubular joints used in tubular truss bridges.

In order to improve the understanding and predictions of the fatigue cracking processes in tubular joints of different sizes, several studies have been carried out at ICOM/EPFL [3, 4, 5, 6] and currently continue. This paper summarises the most recent results obtained.

1.2 Size effects in fatigue

Stated simply, the size effect for welded joints is the phenomenon whereby the fatigue strength of a larger or thicker joint is lower than a smaller or thinner joint of the same geometry, subjected to the same magnitude of stresses. A significant push on research into the size effect in the 1980s provided more convincing evidence, both experimental and analytical, of a trend for lower fatigue strength in thicker specimens of, for the most part, the same geometry [7, 8, 9]. The research work included various types of joint geometries (plate joints, tubular joints), joint preparation (as welded, post-weld heat treated), test conditions (in air, in sea water) and load types (tensile load, bending load). Results from this work led to a few relatively minor modifications and additions to the original Gurney rule [7] given below (formula (1)):

$$\frac{S_{r,T}}{S_{r,Tref}} = \left(\frac{T_{ref}}{T}\right)^{0.25} \quad T_{ref} = \text{reference plate wall thickness} \quad (1)$$

Where $S_{r,T}$ and $S_{r,Tref}$ express the strength as nominal stress ranges for both the plate wall thickness, respectively, the reference plate wall thickness.

In tubular joints, the fatigue size effect is dealt with in analogy to plates in tension with welded details (Gurney rule), namely using a size correction formula (1) in which only the main tube wall thickness appears. The differences with plates is that the hot-spot stress range replaces the the nominal stress range, and the exponent is not a constant, in the formula for tubular joints.

It is recalled here that three factors are generally cited as contributing to the size effect [9, 10, 11]: the statistical size effect, the metallurgical or technological size effect and the geometrical size effect. The latter is often considered as the dominant effect in welded structures. It refers to the through-thickness stress gradient that arises at geometrical discontinuities (e.g. notches) and/or due to bending and torsional loads, which can be addressed by stress analysis. Due to the presence of a steeper stress gradient, a grain close to the surface of a small specimen will experience a lower strain than a grain close to the surface of a thick specimen, for the same stress at the surface.

2 Fatigue tests

2.1 Description of experiments

The test specimens are two uni-planar tubular CHS welded truss beams that were tested under fatigue loading. These beams constitute series S5 (S5 – 1 and S5 – 2) and follow four series using similar specimens previously tested by Schumacher [3, 4]. Truss members are made of steel S355 J2 H conforming to EN10210 – 1:2006 and EN10210 – 2:2006. The nominal dimensions of the specimens are given in *Fig. 1*. Brace members were cut to fit the contour of the chord using computer control technology. Bevels were prepared at angles ranging from 30° to 45°.

Backing-rings were used to facilitate the welder's task and make sure complete penetration of the weld is achieved. A MAG tubular cored metal arc welding with active gas shield (process 136) was used. Non-destructive testing controls of the welds were done by the fabricator following the Swiss code SIA 263/1 [12] rules (requirement: 100 % VT + 50 % UT, for weld quality B, weld quality according to ISO 5817). The test set-up static system corresponded to a simple beam with a concentrated load at mid-span as shown in Fig. 1. Three steel blocks were machined to fit the top chord circular shape with the support blocks and to allow for proper introduction of the load at mid-span.

Weld size has an important effect in the stress concentration at the weld toes of tubular joints. In order to measure the weld size of joints, a mould impression of the welds was done using Rhodorsil RTV 3535 [13]. This modelling material presents very low shrinkage, fast hardening and easiness for application. Real weld dimensions were then compared to the American Welding Society (AWS) recommendations, (*Fig. 2)*.

AWS recommendations are globally fulfilled for both joint 1 and joint 2 and actual weld size is found to be normally much higher then AWS minimum recommendation. Static tests were carried-out in order to: verify the linearity of the loading/unloading response, check symmetry, verify that the out-of-plane bending remains negligible, determine the nominal stress in main joints and evaluate the hot-spot stresses (for specimen S5 – 2).

The fatigue test then started, with periodic stop for NDE and static tests. A sinusoidal fatigue load was applied at a frequency of about 0.7 Hz, with a load ratio $R = Q_{min}/Q_{max}$ of R = 0.1. A single Hydrel 1200 kN (static capacity) actuator under load control was used. The prescribed force range ΔQ= 549 kN, was chosen to obtain the same chord nominal stress range as in previously tested series S3, namely $\Delta\sigma_{nom,ch} = 35$ N/mm^2.

2.2 ACPD system

2.2.1 Application to large-scale truss tests

The ACPD equipment used was developed at ICOM in collaboration with a Swiss manufacturer [14]. Two different acquisition boxes were used, with slightly different characteristics. Compared to other ACPD equipments described in literature, the AC frequency (5 to 6 Hz) is about 10000 lower, but compensated by the introduction of higher intensity of 100 to 150A. The ACPD acquisition box used on specimen S5 – 2 showed improved signal/noise ratio and thus more precise measurement results. In total, 8 (7 for S5 – 1) probes were disposed in potential crack sites corresponding to the crack toe, near imperfections found after visual inspection (*Fig. 3*).

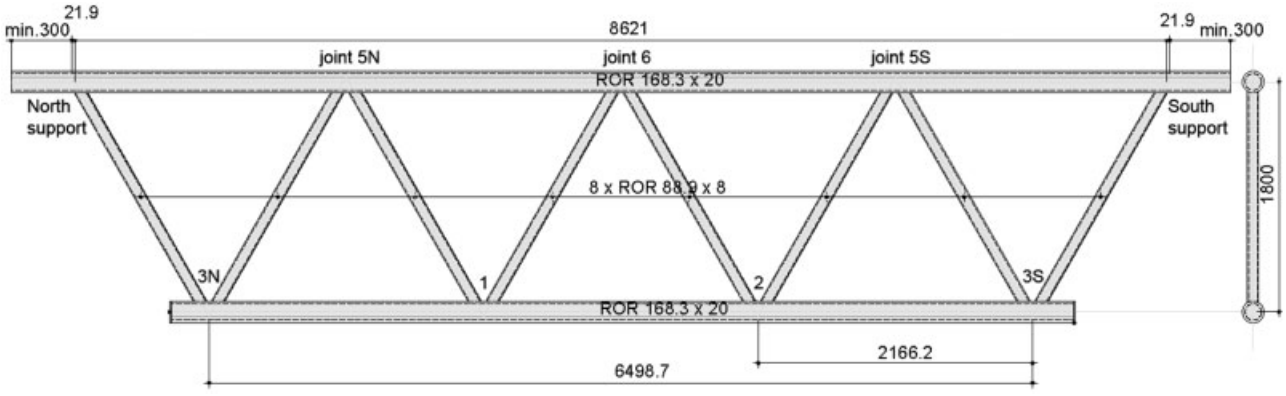

Fig. 1. Elevation of a truss beam with dimensions and joint numbering

Abb. 1. Aufbau des Fachwerkträgers mit Abmessungen und Knotenzahlen

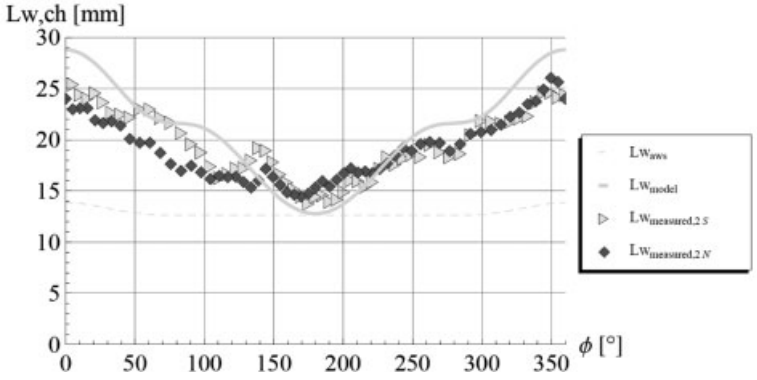

Fig. 2. Comparison of weld leg lengths (footprint) on chord for S5 BEM model, S5 – 2 j2 measured and S5 AWS (2000) recommended minimum

Abb. 2. Vergleich von Schweißschenkel Länge (Fußabdruck) auf Gurt - S5, BEM Modelle, S5 – 2 j2 abgemessen und S5 AWS (2000) empfohlenes Minimum

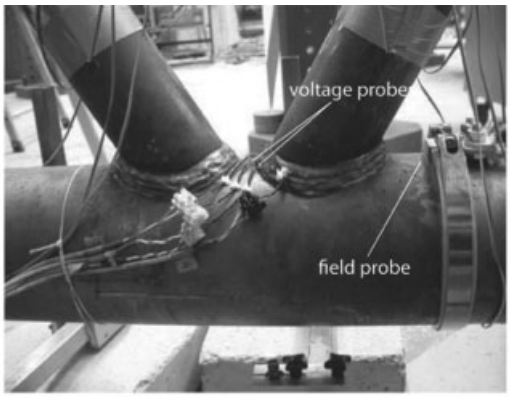

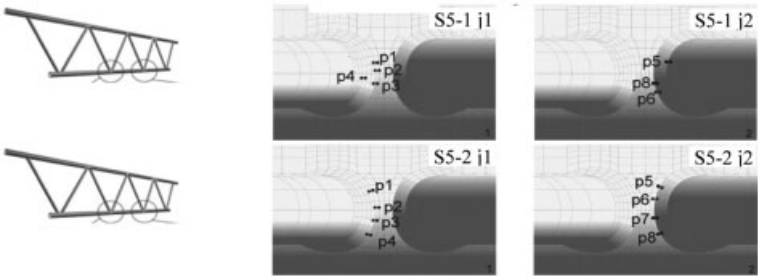

Fig. 3. Alternating current potential drop system – joint with probes (top); Alternating current potential drop probe locations for S5 – 1 and S5 – 2 (bottom)

Abb. 3. Wechselstrom-Potenzial Fall System (ACPD) – Knoten mit Proben (Oben); Wechselstrom-Potenzial Fall Untersuchungsorte für S5 – 1 und S5 – 2 (Unten)

A problem with ACPD estimations in our case is the impossibility to determine through thickness crack penetration. This happens because the depth estimation represents the length along the crack faces and the crack is not vertical but is inclined; and the angle of inclination remains unknown until the joint is opened up. The reported fatigue tests presented two main challenges regarding the use of the ACPD technique: the size and complex geometry (multiple current paths) of the tubular truss.

In order to keep the monitored areas as close to the field probes (primary current introduction) as possible to reduce resistance, only joints j1 and j2 (Fig. 1) were equipped with voltage probes. The actuator and the supports were electrically insulated. Fig. 3 shows one of the joints, the other being the same but with the field probe on the left side of the joint. For beam S5 – 2, to obtain even more information on crack shape and propagation, ink was sprayed into detected cracks. Also, "beach-marks" by different stress amplitude marking were made following the procedure suggested by [15]: Load amplitude is decreased by half, maximum load is kept at the same level, and these loading conditions are applied during 1000 cycles.

2.3 Results

2.3.1 S-N results

The results are expressed in the form of hot-spot stress range, $S_{r,hs}$, versus number of cycles, N. In order to compare the results, one has to define a coherent definition of joint failure. Here, all results are expressed as the life corresponding to complete loss of strength of the joint and identified as N_4. Thus, the test results corresponding to through-thickness cracking were multiplied by a mean factor equal to 1.49 found in previous studies [4, 11]. *Fig. 4* shows the results from these tests, together with the ones from previous similar tests and those from the existing IIW database [11] on CHS joints. The size of the symbols is proportional to the chord thickness, T.

Our new data shows on the graph as two points (test beam S5 – 1 and S5 – 2), but in fact represent a total of 10 fatigue cracks. On both test beams, fatigue cracks were obtained in joints j1, j2, j5N, j5S, and j6. All the cracks occurred at hot-spots 1 or 1c (compression side in the case of elements in compression); for hot-spot locations, *Fig. 5*. It was observed that crack growth, at least up to half the chord thickness, oc-

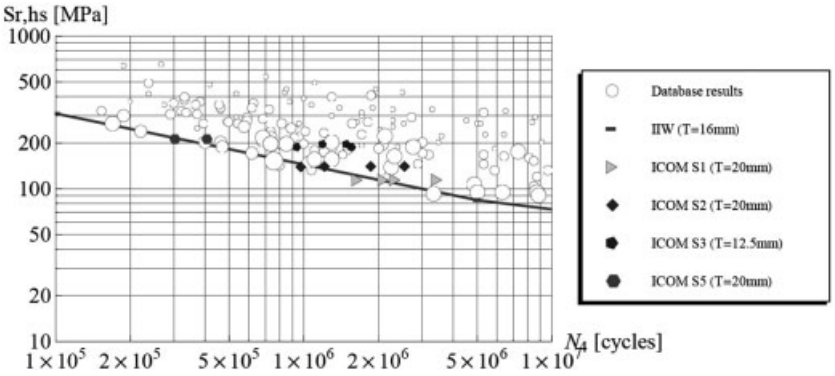

Fig. 4. S-N test results on CHS joints

Abb. 4. S-N Ergebnisse auf kreisformigen Stahlhohlprofilverbindungen (CHS)

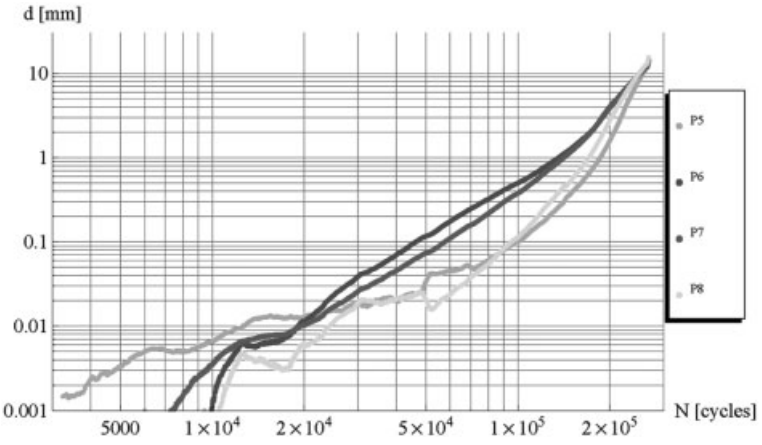

Fig. 5. Stress concentration in the joint (σ_{xx}) - Series S5 fatigue test loading conditions

Abb. 5. Spannungskonzentrationsfaktor im Knoten (σ_{xx}) - Serie S5 unter Ermüdungsversuch Lasten

curred at about the same rate both in tension or compression joints, with crack shapes (*a/c*) being also similar. No crack growth was detected at hot-spot 11 or from the weld root. Size effects were observed when considering all 5 series carried out at ICOM, due to proportional or non-proportional sizing effects between the different series [16].

2.3.2 Crack depth deduced from ACPD

The results can be plotted in terms of crack depth at each probe location, d, in function of the number of cycles. A typical example of the plot is given in *Fig. 6* for joint 2 of beam S5 – 2. One can observe that the first signs of cracking were detected by probe P5, which is on the side of hot-spot 1. However, such small crack sizes can be within the tolerances of the instrumentation. After 20000 cycles, the probes the closest to, besides hot-spot 1, namely P6 and P7, show larger crack depths. But, *Fig. 7*, which shows the comparison between ACPD predicted depths and real crack, confirms the fact that the cracking started from the left side (the side of probe P5). Indeed, the other measurements also showed that the first detectable crack could be on the side of hot-spot 1 (not belonging to the vertical symmetry plane). Also, the first detectable crack happened after less than 10 % of the test fatigue life. All measurements made were stable and with the good results and comparisons obtained, we can say that the size of the specimen and the multiple current paths did not disturb the functioning of the ACPD system.

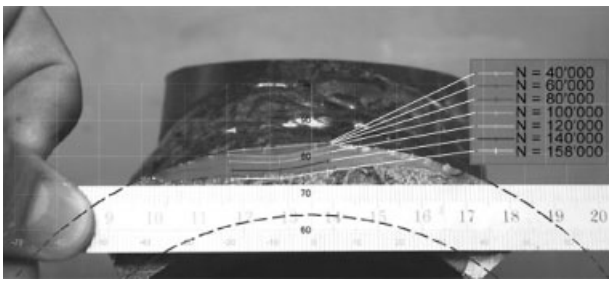

Fig. 6. Number of cycles vs. crack depth for series S5 – 2 joints (filtered results)

Abb. 6. Anzahl Spannungswechsel gegen Risstiefe für Fachwerksknoten S5 – 2 (gefilterte Resultate)

2.3.3 Crack propagation rate

Using the information on the crack depth, one can find the crack propagation rate and plot the results as in *Fig. 8* and *Fig. 9*. For joint S5 – 1, j1, the results from probe P4 are not shown as no propagation was measured (probe at hot-spot 11, Fig. 3). Crack propagation rates from 10^{-7} to 10^{-3} mm/cycle could be measured. The system sensitivity is thus sufficient since, for C-Mn steels, the value 10^{-7} mm/cycle corresponds to stress intensity factor ranges near the threshold value.

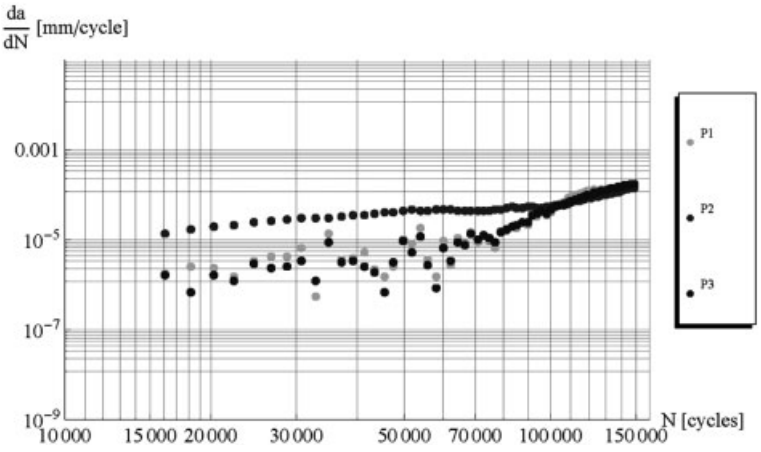

Fig. 7. comparison between ACPD predicted depths and real crack for S5–2, joint j2

Abb. 7. Vergleich zwischen ACPD berechneten Tiefen und echten Risstiefen für S5–2, Knoten j2

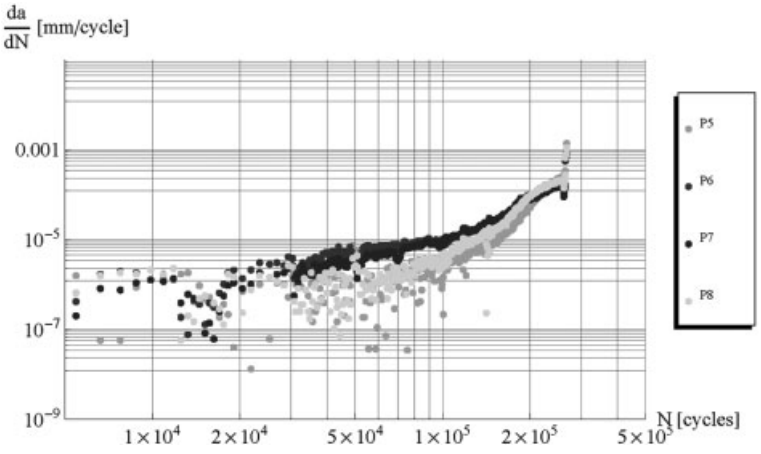

Fig. 8. Crack growth rate vs. number of cycles deduced from ACPD measurement for S5–1, joint j1

Abb. 8. Risswachstumsrate gegen Anzahl Spannungswechsel gefolgert aus ACPD Messungen für S5–1, Knoten j1

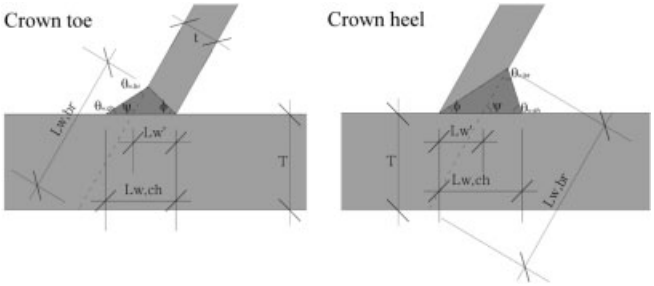

Fig. 9. Crack growth rate vs. number of cycles deduced from ACPD measurement for S5–2, joint j2

Abb. 9. Risswachstumsrate gegen Anzahl Spannungswechsel gefolgert aus ACPD Messungen für S5–2, Knot j2

3 Numerical model

3.1 Introduction

The numerical model objective is the calculation of the stress intensity factors (SIF) for different crack depths with a complex 3D shape. The model presented in the current investigation uses Boundary Elements Method (BEM) commercial code BEASY^{TM} [17]. The crack growth rate is computed using the Paris Law and then the number of cycles to failure is obtained by integration.

3.2 Geometry definition

In order to define the joint model, its boundaries were parametrically defined. The cylinder parametric equation is first used to define the boundaries of chord and diagonals. Then the weld and tubes intersections are defined using the intersection cylinder-cylinder system of equations. Overlapped joints are not considered in this study as they are usually less used in fatigue critical structures (except in mining equipment). *Fig. 10* shows the definition of the different dimensions

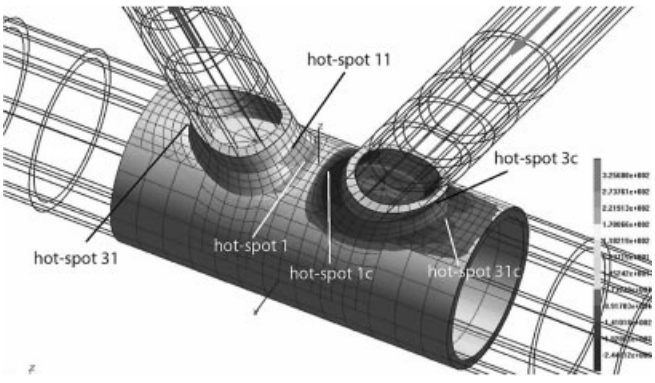

Fig. 10. Dimensions needed to define weld geometry and main geometric parameters

Abb. 10. Erforderliche Dimensionen um Schweißnahtgeometrie und geometrische Hauptparameter zu definieren

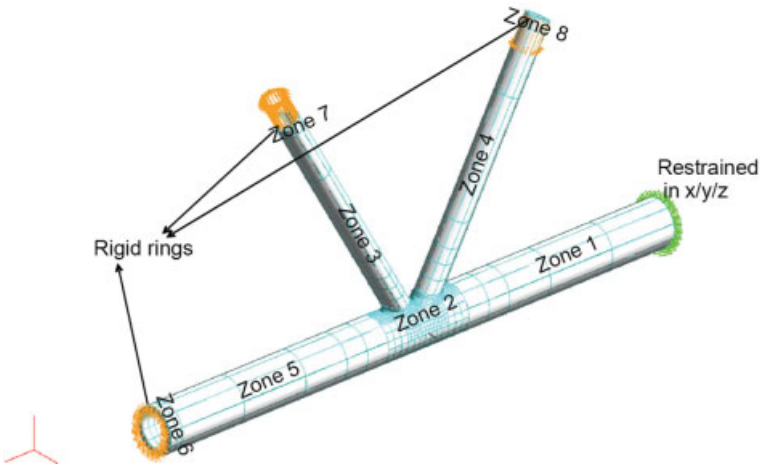

Fig. 11. Zoning of the boundary element model
Abb. 11. Zonen des Randelement-Modells

defining the weld geometry and *Fig. 11* shows the BEM model.

Fig. 2 compares the weld profiles and shows the model is able to closely represent the real weld geometry – as in fatigue test specimen S5 – 2 (joint2) [6, 18]. Both weld profiles respect the AWS requirements. The crack faces belong to the conic surface and the crack front is doubly-curved ([6, 19]). This complex geometry makes modelling of the crack and of the propagation of such a crack in a tubular joint a complicated task, as explained below.

3.3 Meshing

The mesh is a key aspect when performing parametric studies on the influence of changing the size of the structural elements. In the present study, the proportions of the joint elements may change and it is therefore very important to assure that the results reflect the effect of size changes and not the effect of mesh being somewhat different. This was taken care of by doing different validation of the model and of the meshes used:

- by comparing the numerical results to the behaviour of the tested specimen (more details in [6]). This included nominal strains (in the chord and braces), strains in the joint (hot-spot strain) and stress intensity factors for different crack depths , which compared well;
- by model accuracy evaluation from BEASY^{TM} post-processing tools, which showed errors of only 0.01 % within zone 2 (the most important zone, Fig. 11) up to 5 % in zone 6;
- by carrying out mesh convergence tests, which showed the sensitivity of the computed SIF values to the model mesh density. A refined mesh, as the one shown below on Fig. 5, showed to resolve this concern.

As said before, the crack faces belong to the conic surface and the crack front is doubly-curved. This complex geometry makes modelling of the crack and of the propagation of such a crack in a tubular joint a complicated task. The mesh of the crack surface has to be carefully chosen. A good quality mesh depends on the shape of the elements defining the crack surface. Thus, although the software provides a crack growth tool allowing for automatic crack propagation from an initial crack, a manual, stepwise, crack modelling was preferred. The manual crack growth corresponds to the calculation of a set of models with built-in cracks of different given shapes and depths. The crack follows the conic surface and the mesh points are calculated to suit the curved shape. The number of elements and mesh points remains constant for the different crack depths. However BEASY^{TM} automatically remeshes the area near the crack in order to optimally adapt the crack mesh in the existing joint mesh.

3.4 Load cases

A main objective of the present study is to identify the effect of the different basic load cases in the fatigue behaviour of a tubular K-joint. When we consider only the in plane actions, five basic load cases can be isolated. Several considerations justifying the selected method of decomposing the applied forces can be found in [3]. Combined loads results of the simultaneous application of the selected basic cases. Out of the 5 basic load cases, 3 are considered predominant in this study: LC1, LC4 and LC5 (*Table 1*). The developed boundary element model allows for the application of any of the basic cases independently or combined (complex load). A constant nominal stress range is applied and a stress ratio, R, equal to zero or $\sigma_{max} = \Delta\sigma$ is used. Underlying assumption is that there are large tensile residual stresses near the welds and thus practically no crack closure effects.

Table 1. Individual basic load cases and boundary conditions [3]
Tabelle 1. Individuelle grundlegende Lastfälle und Randbedingungen [3]

Load case		Schematic
LC1	Balanced axial brace	
LC4	Axial chord	
LC5	In-plane bending chord	

Table 2. Definition and range of parameters β, γ, τ and T used in the parametric study

Tabelle 2. Definition und Bereich der verwendeten Parameter β, γ, τ und T

β [18]	0.53	0.65			Main geometric parameters:
γ [18]	4.2	7	8.5		β = *d/D* (diameter slenderness)
τ [18]	0.4	0.5	0.6	0.7	γ = *D/2T* (chord slenderness)
T [19]	10	20	40	60	τ = *t/T* (thickness ratio)
					d: outside diameter of the brace *D*: outside diameter of the chord *t*: thickness of the brace *T*: thickness of the chord.

4 Parametric study

4.1 Introduction

The three non-dimensional parameters β, γ and τ were selected as main parametric variables in the study. For each set of non-dimensional parameters, two models with different absolute sizes were run. Joint geometries typical for bridge application (low chord radius to thickness ratio) are selected and the three basic load cases are considered. *Table 2* summarises the range of the parameters covered in the study. A number of other parameters, such as the slenderness α, normalised gap ζ, normalised eccentricity *e/D*, etc. are kept constant during the parametric study but their effects were also evaluated beforehand in an sensitivity analysis.

4.2 Sensitivity analysis

In *Table 3*, the results from the sensitivity analysis are presented. Results are shown and analysed on a "geometry cause"/"effect over the stress intensity factor and fatigue strength" basis. Only two cases result in having a major effect on the stress intensity factor: a change in eccentricity under LC1 (basic load case 1) and a change in chord length under LC5. Theses effects are however mitigated by the way the sizing of the joints was made, for example keeping a sufficient gap for welding, and this can be viewed as inherent technological effects when doing geometrical sizing (i.e. a true practical scaling). In *Table 4*, the trends observed on stress intensity factors values are shown. A strong influence of the geometric parameter τ, i.e. an increase in τ leads to a significant increase in the SIF values is observed for all three basic load cases. The influence of γ is different, it is function of the basic load case considered. Finally β seems to have generally less influence on the SIF values.

Table 3. Trends in the stress intensity factor values obtained from the sensitivity analysis

Tabelle 3. Tendenzen für Spannungsintensitätsfaktor-Werte, erhalten aus der Empfindlichkeitsanalyse

Increase in			
eccentricity, *e*, gap, *g*	↗	↘	↘
chord length, L_{ch}	↔	↔	↗
Truss height, *H*	↔	↔	↔
Weld size, *W*	↘	↗	↘
crack shape, *a/c*	↘	↘	↘
crack angle	↗	↘	↘

↗: minor effect, ↗: major effect

Table 4. Effects of changing β, γ and τ on the stress intensity factor.

Tabelle 4. Wirkungen des Änderns von β, γ und τ auf den Spannungsintensitätsfaktor.

SIF			
τ	↗	↗	↗
β	↘	↔	↔
γ	↗	↘	↘

↗: minor effect, ↗: major effect

In further analyzing the results, a separation is made between the cases where the joint is proportionally sized (true practical scaling) and those non-proportionally sized. In order to compare the results, the geometry correction factor, *Y*, is introduced to normalize the SIF range values, ΔK, using formula (2).

$$Y = \frac{\Delta K}{\Delta\sigma\sqrt{\pi a}} \tag{2}$$

where $\Delta\sigma$ is the applied stress range and *a* is the crack depth. The curve representing *Y*, is found to be well fitted using the relationship given in formula (3).

$$Y = p\left(\frac{a}{T}\right)^{q-1} + \left(\frac{a}{T}\right)^{q} \tag{3}$$

where *p* and *q* are parameters that depend on the geometry and basic load case. Formula (3) ressembles the often used formula $p(a/T)^q$, for example used by Gurney [20], but is found to fit better the BEM results in this study.

4.3 Proportional sizing (or true practical scaling)

When only considering proportional sizing, which means same stress concentration factor (SCF) for both geometries, then the function *Y* of the relative crack depth is common to homothetic joints. The influence of the absolute size of the joint, also known as thickness effect, is determined for the three basic load cases. It is found out that the current size correction formula has a good form, compare equation (1) and (4) below, but the exponent *n* is too detrimental. Values between 0.12 and 0.14 are found from this study.

$$\frac{S_{r,hs,T}}{S_{r,hs,Tref}} = \frac{SCF \cdot S_{nom,T}}{SCF \cdot S_{nom,Tref}} = \left(\frac{T_{ref}}{T}\right)^{n}$$
$$T_{ref} = 16 \text{ mm for CHS accord. to CIDECT} \tag{4}$$

Thus, the value recommended, for proportional sizing, would be $n = 0.14$ for all load cases, instead of values between 0.18 and 0.402 (n being a function of the number of cycles to failure, i.e. $n = 0.06 \cdot \log(N_4)$) as given in CIDECT recommendations [1]. However, proportional sizing in reality seldom occurs. Furthermore, the use of equation (4) would mean as many reference S-N curves as there are different geometries. Thus, to model real problems, it is necessary to consider now non-proportional sizing.

4.4 Non-proportional sizing

When considering non-proportional sizing one can avoid the previous drawback of many reference S-N curves and have only one S-N curve, i.e. one geometry as the reference case. In this study, the following reference geometry is selected:

$$T_{ref} = 16 \text{ mm}, \ \beta_0 = 0.53, \ \gamma_0 = 4.2, \ \text{and} \ \tau_0 = 0.4.$$

In order to uncover the non-proportional sizing effect, the parametric results are analysed focusing again on the geometry correction factor, *Y*. However one makes use of a representative crack depth, a_{rep}, at which the geometry correction factor takes an equivalent through depth value. $Y(a_{rep}/T)$ was determined for each geometry in the parametric study matrix. This approach is similar to the one proposed by Xiao and Yamada [21]. The stress range is calculated at a depth depending on the joint geometry, and load case considered. Thickness effects as well as other geometric size effects (attached tubes and load effects) are encapsulated in both the geometry correction factor and the representative depth at which the stress should be calculated. Detailed information on the $Y(a_{rep}/T)$ procedure is presented in [6]. It is found that the fatigue strength size correction can be expressed as a function of the non-dimensional parameters and load cases as given below.

– For basic load case 1:

$$\frac{S_{nom,(\mathrm{LC1},\beta,\gamma,\tau,T)}}{S_{nom,(\mathrm{LC1},\beta_0,\gamma_0,\tau_0,T_{ref})}} = \left(\frac{T_{ref}}{T}\right)^{0.16} \cdot \left(\frac{\beta_0}{\beta}\right)^{-0.86} \cdot \left(\frac{\gamma_0}{\gamma}\right)^{0.70} \cdot \left(\frac{\tau_0}{\tau}\right)^{0.38} \tag{5}$$

Where $S_{nom,\,LC1,\beta,\gamma,\tau,T}$ is the fatigue strength of the joint with geometric parameters β, γ, τ and T, and $S_{nom,\,LC1,\beta0,\gamma0,\tau0,T0}$ is the reference fatigue strength (or reference S-N curve) for a joint with reference geometric parameters.

– For basic load case 4

$$\frac{S_{nom,(\mathrm{LC4},\beta,\gamma,\tau,T)}}{S_{nom,(\mathrm{LC4},\beta_0,\gamma_0,\tau_0,T_{ref})}} = \left(\frac{T_{ref}}{T}\right)^{0.15} \cdot \left(\frac{\beta_0}{\beta}\right)^{-0.34} \cdot \left(\frac{\gamma_0}{\gamma}\right)^{-0.31} \cdot \left(\frac{\tau_0}{\tau}\right)^{0.44} \tag{6}$$

The results for basic load case 5 are not given here since some correlation between geometrical size and BEM mesh size has been detected. More work still needs to be carried out for this load case.

As it can be seen from formulas (5) and (6), the correction factor for non-proportional sizing depends upon the different geometric parameters β, γ, τ and T but the parameters have different influence, compatible with the trends given in Table 4. Effectively, an increase of one parameter, corresponding to an increase in SIF, means a decrease in fatigue strength or life (according to formulas (5) or (6)). Also, it can be seen that the proportional sizing effect is included within these formulas (term T_{ref}/T) with nearly the same exponent, 0.15 or 0.16 instead of 0.14. This means that, for each basic load and sizing case, the current size correction formula exponent could be lowered to 0.16 (with $T_{ref} = 16$ mm).

Current and future work at ICOM on size effects in fatigue concentrates on the influence on fatigue life and strength of the welding residual stresses, combination of basic load cases and variable amplitude loading.

5 Conclusions

The following conclusions can be drawn from this study:

- All the fatigue cracks occurred at hot-spot 1 and confirm that tubular welded joints for bridge applications show mainly crack propagation because of initial welding imperfections.
- With regard to the influence of welding residual stresses, fatigue cracks were observed both in joints with the chord in tension (joints 1 and 2) as well as in joints with the chord in compression (joints 5N, 5S and 6).
- The ACPD system worked well on those large-scale tubular truss beams and was found very sensitive. It gave precise measurements of the crack depth and also valuable information on crack propagation rates in the range from 10^{-7} to 10^{-3} mm/cycle could be deduced.
- The boundary element method can be used reliably to calculate the stress intensity factors of surface crack with complex shape in CHS joints.
- Results from the numerical model compare well with the experimental measurements (nominal strains, hot-spot strains and stress intensity factors) giving a good estimation of the fatigue life of the joints.
- Proportional and non-proportional sizing can be expressed, for each basic load case, as a function of the non-dimensional parameters and chord thickness (formula (5) and (6)). In all cases, in the current size correction formula, i.e. $(T_{ref}/T)^n$, the exponent could be lowered to $n = 0.16$.

Acknowledgments

The research carried out is part of projects from FOSTA and the Swiss National Science Foundation (SNF). The FOSTA project P591 is supervised by the Versuchsanstalt für Stahl, Holz und Steine at the Technische Universität Karlsruhe, which is supported financially and with academic advice by the Forschungsvereinigung Stahlanwendung e. V. (FOSTA), Düsseldorf, within the scope of the Stiftung Stahlanwendungsforschung, Essen. The SNF support was given for the thesis work of L. Costa Borges under grant no 200021–112014. Other support was given by Vallourec & Mannesmann Tubes, Germany, who provided the tubes for the laboratory tests and Zwahlen & Mayr SA, Switzerland, who fabricated the test specimens.

References

1. X.L. Zhao, S. Herion, J.A. Packer, al., Design guide for circular and rectangular hollow section joints under fatigue loading, *CIDECT, TüV-Verlag Rheinland, Köln*, **2000**.
2. IIW (International Institute of Welding), Fatigue design procedure for welded hollow section joints, *X.L. Zhao and JA Packer (eds.)*, Doc. XIII-1804–99 and XV-1035–99, **2000**.
3. A. Schumacher, Fatigue behaviour of welded circular hollow section joints in bridges, *Ph.D. Thesis*, Thesis EPFL n°2727, Swiss Federal Institute of Technology (EPFL), Lausanne, **2003**.
4. A. Schumacher, A. Nussbaumer, *Engineering Structure*s, **2006**, *28*, 745.
5. S. Walbridge, A. Nussbaumer, *International Journal of Fatigue*, **2007**, *29*, No. 3, 516.
6. L. Costa Borges, Size effects in the fatigue behaviour of tubular bridge joints, *Ph.D. Thesis*, Thesis EPFL n°4142, Swiss Federal Institute of Technology (EPFL), Lausanne, **2008**.
7. T.R. Gurney, Fatigue of Welded Structures, *Cambridge University Press, Cambridge*, **1979**.
8. C. Noordhoek, D.R.V. Van Delft, A. Verhuel, The influence of plate thicknesses on the fatigue behaviour of welded plates up to 160 mm with an attachment or butt weld, *Proceedings SIMS 81*, Elsevier, **1987**, 281–301.
9. O. Örjasäter, Effect of plate thickness on fatigue of welded components. IIW-YWG XIII-XV-118–93, *IIW*, **1995**, 1–19.
10. P.W. Marshall, Design of welded tubular connections, Basis and use of AWS provisions, *Elsevier Science Publishers, Amsterdam,* **1992**.
11. A.M. Van Wingerde, D.R.V. Van Delft, J. Wardenier, J.A. Packer, Scale Effects on the Fatigue Behaviour of Tubular Structures, *WRC Proceedings*, IIW, **1997**.
12. SIA 263/1, Stahlbau - Ergänzende Festlegungen, *Schweizerischer Ingenieur- und Architektenverein*, Zürich, **2003**.
13. Rhodorsil - SIL 01 021 1 : Fiche technique, *Rhodia Chimie - Silicones Europe*, 55 Av. des frères Perret, BP 60, 69192, St-Fons-Cedex, France, **2002**.
14. Mesureur de fissure – 7422, *Lavanchy Electronique*, Av. de la Rochelle 12, CH-1008 Prilly, Switzerland, **2007**.
15. J. Husset, H.P. Lieurade, F. Maltrud, M. Truchon, Fatigue crack growth monitoring using a crack front marking technique, *Welding in the World*, IIW/IIS, Pergamon, **1985**, 276–282.
16. L. Borges, A. Schumacher, A. Nussbaumer, Size effects on the fatigue behaviour of welded CHS bridge joints, *Proc. International Conference on Fatigue and Fracture in the Infrastructure*, Philadelphia, USA, **2006**.
17. BEASY^{TM}, Beasy User Guide, version 9, *Computational mechanics BEASY Ltd,* Ashurst, Southhampton, UK, (http://www.beasy.com), **2005**.
18. A. Nussbaumer, L. Borges, Experimental determination of stress intensity factors on large-scale tubular trusses fatigue tests. *Proc. 12th International Symposium on Tubular Structures (ISTS 12)*, Shanghai, **2008**.
19. L. Borges, A. Nussbaumer, Advanced numerical modelling of fatigue size effects in welded CHS K-joints, *Proc. 12th International Symposium on Tubular Structures (ISTS 12)*, Shanghai, ISTS 12, **2008**.
20. T.R. Gurney, The Influence of Thickness on the Fatigue Strength of Welded Joints, Paper 41, *Proc. of the Second Int. Conf. on Behavior of Offshore Structures*, London, England, 28–31 Aug. **1979**, 523–534.
21. Z.-G. Xiao, K. Yamada, *International Journal of Fatigue*, **2004**, *26*, 1277.

Corresponding author: A. Nussbaumer, Steel Structures Laboratory – ICOM, Station 18, École Polytechnique Fédérale de Lausanne, EPFL, CH-1015 Lausanne, Switzerland, E-mail : alain.nussbaumer@epfl.ch

Received in final form: August 26, 2008 [T 356]